# Rotation Detection in Chest Radiographs based on Generalized Line Histogram of Rib-Orientations

K.C. Santosh†, S. Candemir†, S. Jaeger†, L. Folio‡, A. Karargyris†, S. Antani†, G. Thoma†
†Communications Engineering Branch
US National Library of Medicine (NLM), National Institutes of Health (NIH)
8600 Rockville Pike, Bethesda, MD 20894, USA

‡Department of Radiology and Imaging Sciences
Clinical Center, National Institutes of Health (NIH)
Bethesda, MD 20892, USA,

Email: {santosh.kc, sema.candemir, stefan.jaeger, les.folio, alexandros.karargyris, sameer.antani, george.thoma}@nih.gov

***Abstract*—We present a generalized line histogram technique to compute global rib-orientation for detecting rotated lungs in chest radiographs. We use linear structuring elements, such as line seed filters, as kernels to convolve with edge images, and extract a set of lines from the posterior rib-cage. After convolving kernels in all possible orientations in the range $[0, \pi)$, we measure the angle for which the line histogram has maximum magnitude. This measure provides a good approximation of the global chest rib-orientation for each lung. A chest radiograph is said to be upright if the difference between the orientation angles of both lungs with respect to the horizontal axis, is negligible. We validate our method on sets of normal and abnormal images and argue that rib orientation can be used for rotation detection in chest radiographs as aid in quality control during image acquisition, and to discard images from training and testing data sets. In our test, we achieve a maximum accuracy of 90%.**

***Index Terms*—Chest radiographs; generalized line histogram; rib-orientations; rotation detection.**

## I. Introduction

Quality control is a critical issue when large number of digital chest radiographs (or chest X-ray (CXR)) need to be acquired in an automated fashion, such as during mass population screening [1]. For this, images need to be inspected for proper x-ray penetration, adequate inspiration (inhaling) by the patient, proper angulation, and importantly, the image should be devoid of any rotation. Rotation can adversely affect the performance of subsequent automated processing steps in screening algorithms or computer-aided diagnosis, such as lung segmentation [2]. Further, rotation can also affect one-to-one zone comparison, viz. upper, middle, and lower between lung sections. While rotated CXRs may not necessarily be challenging for radiologists, they can confuse the machine that is operating in either a computer-assisted or a fully-automated fashion. An automatic method for detecting rotated images is desirable to enable machines to reject the rotated CXR and/or forward it to a human operator for closer inspection. Rotation in CXRs can often be expected for images acquired with portable machines in non-hospital settings or under more challenging outdoor conditions, such as mobile screening stations in rural areas. In addition to pathology-related rotations, misaligned body positions are more frequent in these cases due to hardware limitations of the screening setup used, poorly-observed screening protocols, or other factors [3], [4].

To acquire an upright CXR, a radiology technician needs to align the patient's body so that it is perpendicular to the x-ray beam. Any deviation from this position will result in a rotated image. The degree of rotation in a CXR can be computed by analyzing the relationship of the medial heads of the clavicles to the adjacent spinous processes in the upper thorax. Normally, the spinous processes lie equidistant from the medial heads of the clavicles. From a practical point of view, the automatic detection of clavicle heads and spinous processes needs to be precise. Even a small deviation of 10 to 20 pixels (in and out) with respect to the actual boundary, can adversely affect the decision process. We observe that radiologists can reliably decide if a CXR is rotated by using other contextual information independent of the clavicles. Motivated by this, we detect rotation based on the rib-orientation. A rotated lung is likely to affect the positions of clavicles and ribs in the same way. In addition, this method is likely to be more stable because the number of ribs is relatively high and the entire rib-cage can be used.

Humans have 12 pairs of ribs including false and floating ribs [5]. Not all of these ribs are necessarily visible in a typical radiograph for various reasons. However, the visible subset is usually sufficient to compute the global rib-orientation. Very few papers on rib detection and segmentation methods have been reported in the literature [6]–[9]. However, the published methods usually do not detect the false and floating ribs. Further some methods detect the ribs only partially due to the large variation of intensity distributions in CXRs. It is interesting to note that computing the rib-vertebra anglei.e., the angle between a rib and its corresponding vertebra, which is a clinically accepted method [10], [11]. These works used radiographs of scoliosis patients for which they computed the rib-vertebra angle difference (RVAD), for all ribs. Similarly, image registration method for interval change detection between two CXRs based on the difference in anterior-posterior inclination angles has been reported [12]. Due to low accuracy in rib and

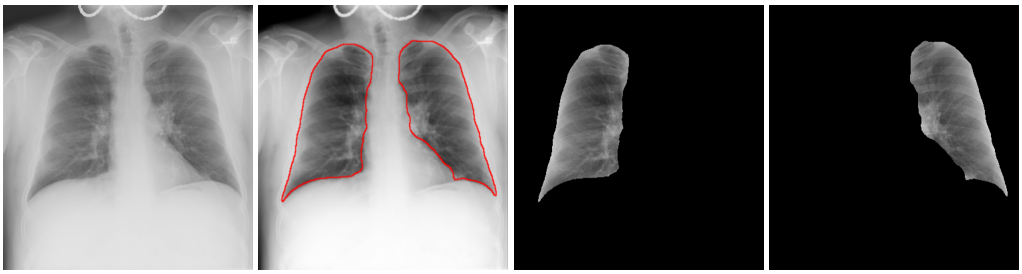

(a) Input image (b) Lung segmentation (c) Right lung (d) Left lung

Fig. 1. An example showing the complete process of segmenting lung sections (right and left) using graph-cut algorithm.

vertebra segmentation, we propose a method for computing the *global* rib-orientation for both lungs. Missing a pair of ribs does not negatively affect the output of this method because we are only interested in the global rib-orientation and not in the orientation of individual ribs. Contributions of our work to the science are: 1) we have developed a generalized line histogram method to compute rib-orientations; and 2) we apply this method as a decision making tool for rotation detection and quality control in acquisition of CXRs, particularly in remote rural areas during mass population screening. Taking rotation into account using ribs minimizes false positive detection caused by overlapping densities in a rotated patient.

The remainder of this paper is organized as follows. We start with detailing our proposed method in Section II. This includes lung segmentation, line seed filter (kernel) development, line histogram computation, and rotation decision. In Section III, we evaluate the approach. We conclude the paper in Section IV with a summary of our results.

## II. The Proposed Method

### A. Lung section segmentation

To effectively compute the rib-cage edge distribution, it is necessary to segment right and left lung sections from the whole image. There are several state-of-the-art algorithms, to detect the lung regions. In this work, we use our algorithm which is based on graph-cut algorithm guided by patient-specific atlas model [13]. The system first builds a subset of atlases (which are expert delineation of lung boundaries of several patients) by choosing the most similar x-rays in terms of shape similarity of lungs. Then, it warps these selected atlases to the target CXRs using a registration algorithm. We use the scale invariant feature transform (SIFT) flow (i.e., SIFT-flow) registration approach [14] which computes the corresponding pixels of image pairs according to their SIFT feature similarity. The spatial difference between the corresponding pixels is used to warp the masks derived from training CXRs to build a lung model for the target CXR. The lung model and intensity information of the target CXR are combined by using the objective function: data term, smoothness term and lung model term. The data term forces the segmentation suitable to intensity information of the CXRs; the smoothness term produces a smooth solution; and the model term guides the algorithm to produce a segmentation result similar to the patient lung model. The final lung boundary is computed by solving the objective function with graph cut energy minimization approach [15]. Fig. 1 shows a couple of output examples of it, where the detected right and left lung sections are separately illustrated.

### B. Generalized line histogram

#### B.1 Kernels.

To detect key lines from the image, we define line seed filter kernels that is defined in a normal Gaussian distribution. We compute probability density function (pdf) at each of the values in $X$ using the normal distribution,

$$\mathbf{f}\left(x,\mu,\sigma\right)=\frac{1}{\sigma\sqrt{2\pi}}exp\left(\frac{-(x-\mu)^2}{2\sigma^2}\right), \tag{1}$$

where $\sigma = 1$, $\mu = 0$ and $X$ is a vector and its values are confined in the range $[-\sigma, \sigma]$. To make it simple, in the discrete case, a structuring element can be represented as a set of pixels on a grid, assuming the values 1 if the pixel belongs to the structuring element or 0, otherwise [16], [17]. Based on this, we define a binary kernel representing a line of any particular length $len$ and angle $\theta$ i.e., $\mathbf{f}\left(`line', len, \theta\right)$. To generate a kernel that represents the shape of a Gaussian ('bell-shaped') hump $g$, we perform an element-wise multiplication of binary kernel with the values obtained from Eq. (1),

$$g=\mathbf{f}\left(`line', len, \theta\right)\circ\mathbf{f}\left([-\sigma:\frac{2\sigma}{len-1}:\sigma],\mu,\sigma\right). \tag{2}$$

Note that the kernel size depends on the length of the linear structuring element. Unsurprisingly, larger the size of the kernel matrix, lesser the number of lines.

Considering a set $\Theta$ of possible different orientations $\{\theta_k\}$ which are specified in the range $[0°, 180°)$, we have a set $\mathcal{K}$ of kernels $\{g_k\}$,

$$\mathcal{K}=\{g_k\}_{k=1,\ldots,K},\ \text{and}\ \theta_k=\frac{180°}{bin_k}(k-1), \tag{3}$$

where $bin$ is the number of bins and the index $k$ associated with kernel $g$ determines the orientation value i.e., $\theta_k$.

#### B.2 Line histogram.

Given an edge image $edg(m, n)$ of size $M \times N$, our idea is to perform convolution with the kernel $gK$. Note that the edge image is resulted from Canny edge detector after

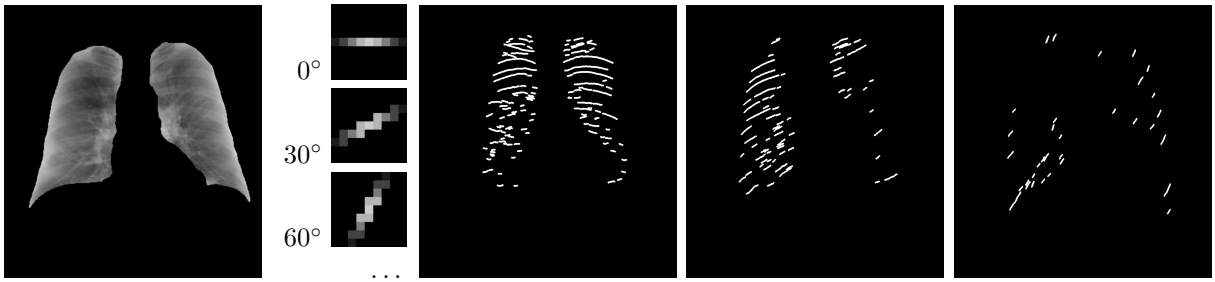


(a) Masked lungs (b) Kernels (c) Line output at 0 (d) Line output at 30° (e) Line output at 60

Fig. 2. An example showing (a) lung sections (*cf.* Fig. 1), (b) kernels at three different orientations, which are defined in 1D Gaussian distribution and (c-e) the corresponding lines that are via convolution.

global histogram equalization. Convolution in general, can be expressed as $o(m,n) = g \otimes edg$

$$o(m,n) = \sum_{i=1}^{I} \sum_{j=1}^{J} g(i,j) edg(m-i, n-j). \quad (4)$$

This means that, for each pixel $(m,n)$ in the image, the convolution output value $o(m,n)$ is calculated by translating the convolution mask to pixel $(m,n)$ in the image, and then taking the weighted sum of the pixels in the neighborhood about $(m,n)$, where the individual weights are the corresponding values in the convolution mask. Such a convolution produces prominent lines that are appeared in the lung section. Consider a complete set $\mathcal{K}$ of kernels (*cf.* Eq. (3)), convolution will produce a complete set $\mathcal{L}$ of lines, $\mathcal{L} = \mathcal{K} \otimes edg = \{\ell_k\}_{k=1,\ldots,K}$, where $\ell_k$ refers to the set of lines in that particular index $k$. Fig. 2 shows a few examples of it. Formally, any $\ell$ can be represented by a tuple: total number of lines ($noL$) and total length of the lines ($loL$) i.e., $\ell = \langle noL, loL \rangle$.

To compute histogram, without loss of generality, we use $loL$ in every particular $k$ since lengths of the lines vary from one line to another (see Fig. 2). Based on this, a complete set $\mathcal{H}$ of line histograms $h_k = loL_k$ of lines in every convolution, designated by kernel $g_k$ is

$$\mathcal{H} = \{\hbar_k\}_{k=1,\ldots,K}, \text{ and } \hbar_k = \frac{1}{\max(h_k)} h_k. \quad (5)$$

### C. Chest radiograph rotation

Global chest rib-orientation can be computed as, $\arg\max_k(\hbar_k)$ i.e., the angle from which the maximum magnitude of line histogram is produced.

Consider two lung sections: right and left, and kernels at several different $\theta$ values from $0°$ to $180°$, the CXR is said to be upright if their orientation angle difference $\Delta$ is zero or negligible (see Fig. 3), $\Delta_{\alpha_{1,2}} = |\alpha_1 - \alpha_2| \approx 0$, where $\alpha_1 = \theta_1$ and $\alpha_2 = 180 - \theta_2$ respectively represent the global chest rib-orientation angles from right and left lung sections. In practical, since $\Delta_{\alpha_{1,2}} \neq 0$, our decision relies on a small tolerance (tol.) to perform a binary response. Therefore, the proposed algorithm accepts the test CXRs as rotated ones if $\Delta_{\alpha_{1,2}} \geq \Delta^{tol.}_{\alpha_{1,2}}$ and rejects them as non-rotated ones, otherwise. In our test, $\Delta^{tol.}_{\alpha_{1,2}}$ is empirically designed based on the observations.

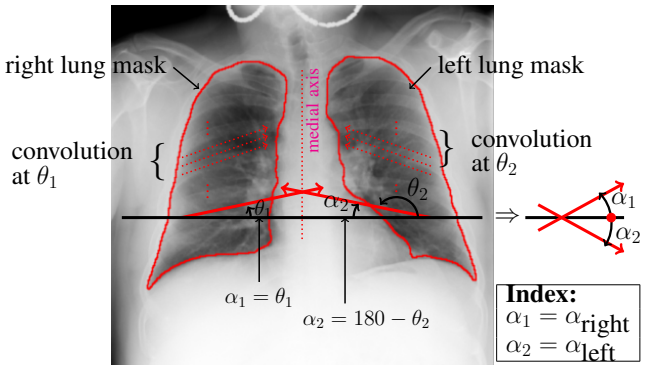


Fig. 3. An example (*cf.* sample 1 in Fig. 1), illustrating the way to compute CXR rotation based on global rib-orientations, by separately taking two lung sections.

## III. Validation

### A. Dataset, ground-truths and evaluation protocol

Two different datasets: Indiana and Montgomery county, are used in our test. The Indiana dataset is a large collection of over 4000 frontal CXRs covering a wide range of lung abnormalities. The images were acquired as a part of routine clinical care at a university hospital and a regional hospital affiliated with the Indiana University School of Medicine. From this, we have selected all rotated (50 samples) and a subset of 100 non-rotated samples. The Montgomery dataset contains 138 frontal CXRs, where several abnormal CXRs show manifestations of Tuberculosis and have abnormal lung shapes. The images were acquired within the tuberculosis control program of the Department of Health and Human Services of Montgomery County in Maryland, USA. Both datasets have been de-identified at source and are exempted by the respective IRBs at the source organizations and the National Institutes of Health. Since it is hard to provide an accurate rotation angle for the expert, our evaluation protocol follows binary (1|0) classification: rotated or non-rotated i.e., qualitative response. In our testing protocol, the response returned from our algorithm is correct if it matches the expert's response.

For evaluation, considering whole dataset size $B$, we compute accuracy of the algorithm's response (AR) with respect

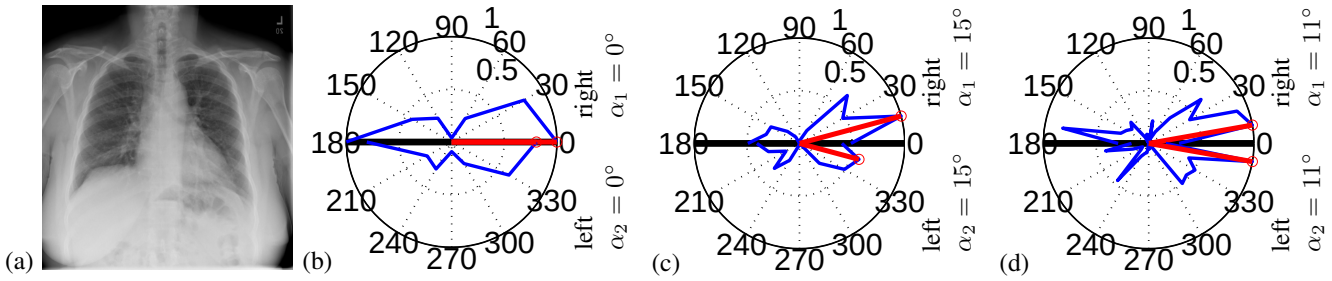


Fig. 4. An example showing line histograms from (a) a chest radiograph in three different number of bins: (b) 6 (at 30° see Fig. 2), (c) 12 (at 15°) and (d) 180 (at 1°), for making decisions. The sample, taken from the Indiana dataset has been decided as fully up-right chest radiograph. As an example, rib-orientation angle difference $\Delta_{\alpha_{12}} = |11° - 11°| = 0$ when $bin = 180$.

to the expert's response (ER) as,

$$\text{accuracy} = \frac{\sum_{b=1}^{B} \text{AR}_b \cap \text{ER}_b}{\text{B}}, \tag{6}$$

where $\text{AR} \cap \text{ER} = 1$ if $\text{AR} = \text{ER}$ and 0, otherwise. Note that the responses: ER and AR are just binary sequences i.e., $\text{ER}_b, \text{AR}_b \in \{0, 1\}$.

### B. Observations and analysis

Before reporting an overall performance of our algorithm, we first illustrate its operation through an example shown in Fig. 4. Here,

1) the solid horizontal line (in black) separates the line histograms from right and left lung sections; and
2) different number of bins are employed to see whether decision changes.

We remind the reader that the number of bins depends on the convolution angle interval (*cf.* Eq. (3)). In this example, for different number of bins viz. 6, 12 and 180, $\Delta_{\alpha_{1,2}}$ is zero regardless their separate values. This provides the fact the decision remains unchanged (i.e., up-right chest radiograph) even when number of bins vary. At the same time, while observing the histogram's precision, we keep $1°$ angular step for convolution. Considering the whole dataset, we have achieved a maximum accuracy of 90% (from Montgomery county dataset) at an average rate of 1.2 seconds per CXR using MATLAB 2013a in Linux platform (see Table I).

In what follows, we discuss the following issues, such as

1) accuracy,
2) precision in rib-orientation, and
3) convolution angle-range.

Accuracy has been degraded by non-rotated samples as well as slightly rotated samples. Beside large variation in intensity distribution, it is primarily because of the hard threshold (i.e., tolerance) in decision making. We have noted that there exists always a small rib-orientation angle difference even from the up-right CXR. As a consequence, smaller threshold i.e., $\Delta^{tol.}_{\alpha_{12}} = 5°$ may not correctly separate non-rotated CXRs from rotated ones. On the other hand, threshold increment (up to $10°$) offers satisfactory results since it can distinguish severely rotated and non-rotated samples, which is an interesting part of the paper, while slightly rotated samples are still not correctly verified. As an example, in Fig. 5, our algorithm responds that all samples are rotated when $\Delta^{tol.}_{\alpha 12} = 5°$. But samples 1, 5 and 6 are not considered as rotated when $\Delta^{tol.}_{\alpha 12} = 10°$.

TABLE I
PERFORMANCE EVALUATION.

| | Indiana | Montgomery |
|---|---|---|
| Accuracy@$\Delta^{tol.}_{\alpha_{1,2}}$ | 79%@5° | 83%@5° |
| | 84%@10° | 92%@10° |
| CXR sample size | 4020×4892 pixs. (scaled down to 0.25) | |
| Running time | 1.2 sec/sample when $bin = 180$ (system: MATLAB 2013a in Linux) | |

While mathematical formulation allows all possible angles from $0° - 180°$, practical implementations do not need to compute beyond $60°$. This helps reduce the running time to 1.2 seconds per CXR as reported in Table I.

## IV. Summary and Futher Work

In this paper, we have presented a method for detecting rotation in frontal chest radiographs by developing a generalized line histogram based rib-orientation detector. The method uses a line seed filter kernel to convolve with an edge image that produces a set of lines in several different possible directions.The angle from which the magnitude of the histogram is maximum refers to the global rib-orientation angle. Considering both (left and right) lung sections, from our experimental tests, we have observed that the proposed method can distinguish severely rotated CXRs from non-rotated ones, and achieved a maximum overall accuracy of 92%.

In this prototype effort, our decision is based on a hard threshold. It is possible to learn an optimal threshold from various training samples reviewed by an experts. However, the number of available rotated images are few since many are eliminated during acquisition quality control.

## Acknowledgements

This research was supported [in part] by the Intramural Research Program of the National Institutes of Health (NIH),

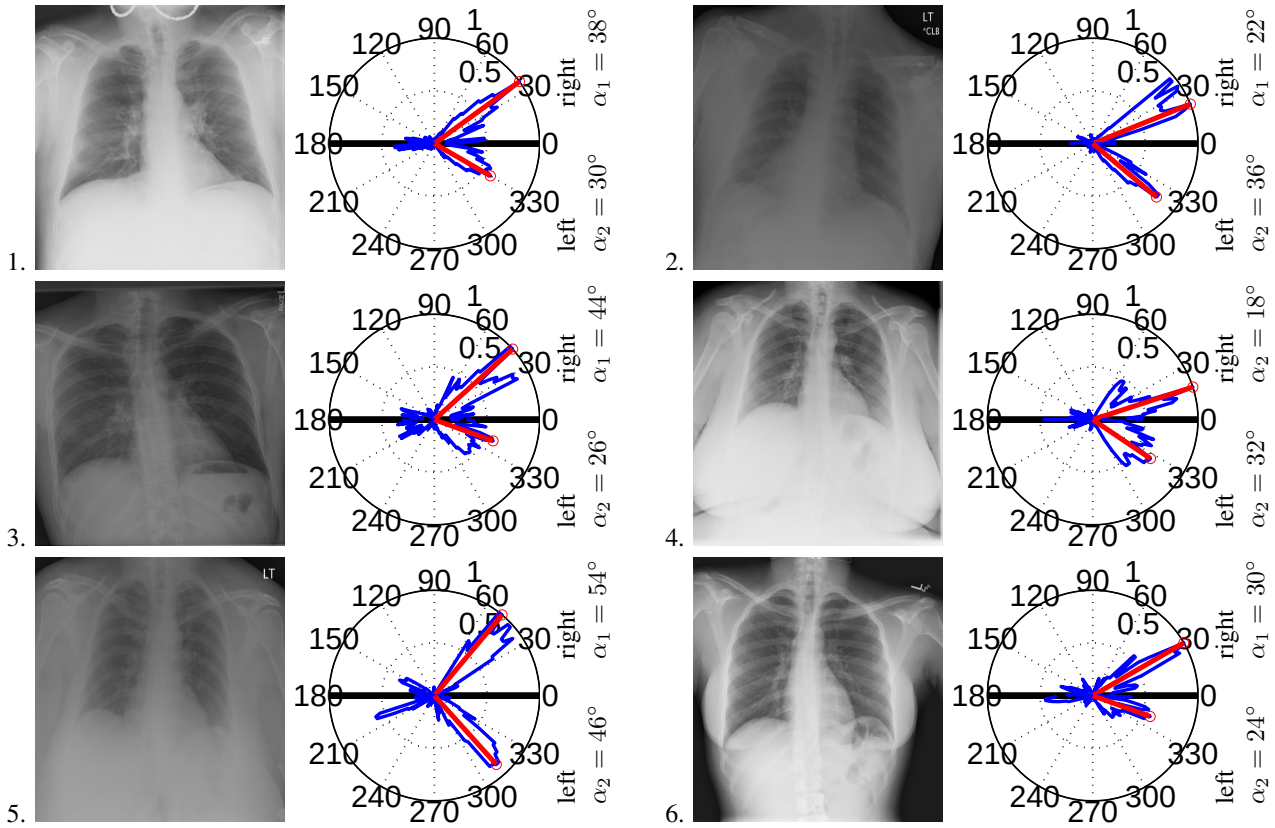


Fig. 5. A few examples illustrating whether CXRs are rotated based on global chest rib-orientation, when taking tolerance, $\Delta_{\alpha 12}^{tol.} = 5°$.

National Library of Medicine (NLM), and Lister Hill National Center for Biomedical Communications (LHNCBC).

## REFERENCES


[1] S. Jaeger, A. Karargyris, S. Candemir, L. Folio, J. Siegelman, F. Callaghan, Z. Xue, K. Palaniappan, R. Singh, S. Antani, G. Thoma, Y.-X. Wang, P.-X. Lu, and C. J. McDonald, "Automatic tuberculosis screening using chest radiographs," *IEEE Trans. on Medical Imaging (to appear)*, 2014.

[2] D. K. Iakovidis, M. A. Savelonas, and G. Papamichalis, "Robust model-based detection of the lung field boundaries in portable chest radiographs supported by selective thresholding," *Meas. Sci. Technol*, vol. 20, no. 10, 2009.

[3] F. Bongard, D. Sue, and J. Vintch, *Current Diagnosis and Treatment Critical Care*. McGraw-Hill Education, 2008.

[4] S. Jaeger, A. Karargyris, S. Candemir, J. Siegelman, L. Folio, S. Antani, G. Thoma, and C. J. McDonald, "Automatic screening for tuberculosis in chest radiographs: a survey," *Quantitative Imaging in Medicine and Surgery*, vol. 3, no. 2, 2013.

[5] K. S. Saladin, *Anatomy & physiology: the unity of form and function*. McGraw-Hill, 2010.

[6] H. Wechsler and J. Sklansky, "Automatic detection of rib contours in chest radiographs," in *International Joint Conference on Artificial Intelligence*, 1975, pp. 688–694.

[7] H. Wechsler, *Automatic detection of rib contours in chest radiographs: an application of image processing techniques in medical diagnosis*, ser. Interdisciplinary systems research. Birkhäuser, 1977.

[8] P. de Souza, "Automatic rib detection in chest radiographs." *Computer Vision, Graphics, and Image Processing*, vol. 23, no. 2, pp. 129–161, 1983.

[9] A. Karargyris, S. Antani, and G. Thoma, "Segmenting anatomy in chest x-rays for tuberculosis screening," in *Annual International Conference of the IEEE Engineering in Medicine and Biology Society*, 2011, pp. 7779–7782.

[10] M. H. Mehta, "The rib-vertebra angle in the early diagnosis between resolving and progressive infantile scoliosis," *Journal of Bone and Joint Surgery - British Volume*, vol. 54, no. 2, pp. 230–243, 1972.

[11] T. B. Grivas, R. G. Burwell, M. Purdue, J. K. Webb, and A. Moulton, "Segmental patterns of rib-vertebra angles in chest radiographs of children: Changes related to rib level, age, sex, side and significance for scoliosis," *Clinical Anatomy*, vol. 5, no. 4, pp. 272–288, 1992.

[12] Y. Matsuo, A. Shimizu, and H. Kobatake, "An interval change detection method for two chest x-ray images with different rotation angles of the human body and its performance evaluation," *Systems and Computers in Japan*, vol. 36, no. 10, pp. 30–42, 2005.

[13] S. Candemir, S. Jaeger, J. Musco, Z. Xue, A. Karargyris, S. Antani, G. Thoma, and K. Palaniappan, "Lung segmentation in chest radiograps using anatomical atlases with non-rigid registration," *IEEE Trans. on Medical Imaging (to appear)*, 2014.

[14] C. Liu, J. Yuen, and A. Torralba, "SIFT flow: Dense correspondence across different scenes and its applications." *IEEE Trans. Pattern Anal. Mach. Intell.*, vol. 33, no. 5, 2011.

[15] Y. Boykov, O. Veksler, and R. Zabih, "Fast approximate energy minimization via graph cuts," *IEEE Transactions on Pattern Analysis and Machine Intelligence*, vol. 23, no. 11, pp. 1222–1239, 2001.

[16] J. Serra, *Image Analysis and Mathematical Morphology*. Orlando, FL, USA: Academic Press, Inc., 1983.

[17] C. Hendriks and L. Vliet, "Discrete morphology with line structuring elements," in *International Conference on Computer Analysis of Images and Patterns*, ser. Lecture Notes in Computer Science, N. Petkov and M. Westenberg, Eds. Springer Berlin Heidelberg, 2003, vol. 2756, pp. 722–729.